HHS Public Access

Author manuscript

FASEB J. Author manuscript; available in PMC 2023 November 01.

Published in final edited form as:

FASEB J. 2022 November ; 36(11): e22567. doi:10.1096/fj.202200558R.

Gene Dosage Changes in *KCTD13* Result in Penile and Testicular Anomalies Via Diminished Androgen Receptor Function

Abhishek Seth[1,2,5], **Armando Rivera**[1,2], **In-Seon Choi**[1,2], **Olga Medina-Martinez**[1,2], **Shaye Lewis**[1,2], **Marisol O'Neill**[2,3], **Alex Ridgeway**[2], **Joshua Moore**[2], **Carolina Jorgez**[1,2], **Dolores J. Lamb**[1,2,3,4]

[1]Scott Department of Urology, Baylor College of Medicine, Houston, TX, 77030.

[2]Center for Reproductive Medicine, Baylor College of Medicine, Houston, TX, 77030.

[3]Department of Molecular and Cellular Biology, Baylor College of Medicine, Houston, TX, 77030.

[4]The James Buchanan Brady Foundation Department of Urology, Center for Reproductive Genomics and Englander Institute for Personalized Medicine, Weill Cornell Medical College.

[5]Department of Surgery, Nemours Children's Hospital, Orlando, Florida 32827

Abstract

Despite the high prevalence of hypospadias and cryptorchidism, the genetic basis for these conditions is only beginning to be understood. Using array-comparative-genomic-hybridization (aCGH), *potassium-channel-tetramerization-domain-containing-13* (*KCTD13)* encoded at 16p11.2 was identified as a candidate gene involved in hypospadias, cryptorchidism and other genitourinary (GU) tract anomalies. Copy number variants (CNVs) at 16p11.2 are among the most common syndromic genomic variants identified to date. Many patients with CNVs at this locus exhibit GU and/or neurodevelopmental phenotypes. *KCTD13* encodes a substrate-specific adapter of a BCR (BTB-CUL3-RBX1) E3-ubiquitin-protein-ligase complex, which has essential roles in the regulation of cellular cytoskeleton, migration, proliferation, and neurodevelopment; yet its role in GU development is unknown. The prevalence of *KCTD13* CNVs in patients with GU anomalies (2.58%) is significantly elevated when compared to patients without GU anomalies or in the general population (0.10%). *KCTD13* is robustly expressed in the developing GU tract. Loss of *KCTD13* in cell lines results in significantly decreased levels of nuclear androgen receptor (AR), suggesting that loss of *KCTD13* affects AR sub-cellular localization. *Kctd13* haploinsufficiency and homozygous deletion in mice cause a significant increase in the incidence of cryptorchidism and micropenis. *KCTD13*-deficient mice exhibit testicular and penile

Address correspondence to: Dolores J. Lamb, Ph.D., Weill Cornell Medicine, Urology, 525 E 68th Street, Box 94 New York, NY 10065 Telephone: 212-746-4618. Fax: 646-962-0190. dlamb@med.cornell.edu, Abhishek Seth, 6535 Nemours Parkway, Orlando, Florida, 32827. Telephone: 302-304-9789. Fax:407-650-7266. abhishek.seth@nemours.org.

Author Contributions

A Seth, C Jorgez and D Lamb designed research; A Rivera, A Ridgeway, I Choi, O Medina-Martinez, S Lewis, C Jorgez, J Moore, A Seth, M O'Neill analyzed data; A Rivera, A Ridgeway, I Choi, O Medina-Martinez, S Lewis, C Jorgez, J Moore, A Seth, M O'Neill performed research; A Seth, C Jorgez and D Lamb wrote the paper; A Seth and D Lamb contributed new reagents or analytic tools.

Conflict of Interest Statement

The authors have stated explicitly that there are no conflicts of interest in connection with this article.

abnormalities together with significantly reduced levels of nuclear AR and SOX9. In conclusion, gene-dosage changes of murine *Kctd13* diminish nuclear AR sub-cellular localization, as well as decrease SOX9 expression levels which likely contribute in part to the abnormal GU tract development in *Kctd13* mouse models and in patients with CNVs in *KCTD13*.

Keywords

KCTD13; copy number variant (CNV); cryptorchidism; penile anomalies

INTRODUCTION

Congenital anomalies of the genitourinary (GU) tract are a common occurrence that arise from disturbances during embryonic development. These GU anomalies can range from hypospadias, improper positioning of the urethral opening on the ventral side of the penis, to complete phenotypic sex reversal. Hypospadias occurs in 1 of 125 live births, and sexual ambiguity occurs in 1 of 2000–4500 children[1,2]. Cryptorchidism, or undescended testis (UDT), is the most common GU birth defect, occurring in 3% of full-term infants[3]. Despite the high prevalence of congenital GU defects, their underlying molecular mechanisms are only now beginning to be understood. GU anomalies in humans are attributed to both gene mutations and structural chromosomal abnormalities (3–18). Genomic hotspots for copy number variants (CNVs), caused by uneven meiotic crossover resulting in the loss or gain of one or more gene copies at a particular locus, provide insight into regions encoding genes required for normal GU development (3–20). Array comparative genomic hybridization (aCGH) revealed that these genomic microdeletions and microduplications are present in about 21.5% of patients with congenital GU defects diagnosed as non-syndromic[4]. One such hotspot for GU anomalies is the locus at 16p11.2[4–7]. 16p11.2 is a very heterogeneous locus with high genomic complexity and incomplete penetrance as many individuals carrying this rearrangement appear phenotypically normal. However, some of these individuals will have clinical phenotypes that include high incidences of neurodevelopmental and GU defects such as: cryptorchidism, hypospadias, micropenis, and congenital anomalies of the kidney and urinary tract (CAKUT)[4–14].

A subset of patients with hypospadias and cryptorchidism displayed an increased incidence of CNVs at 16p11.2[4,7]. Using this data, we tested the hypothesis that due to the presence of both upper and lower GU defects in this region there are at least two dosage-sensitive genes in this region, one which is required for normal virilization of the male external genitalia since both testicular descent and penile development are impaired, and the other for CAKUT defects. Our group recently identified that the dosage-sensitive gene in this minimal region affecting upper tract development resulting in CAKUT, is *MAZ*[7]. *KCTD13*, a gene identified by locus mapping in the minimal region identified, was selected as a plausible candidate gene for lower GU anomalies at 16p11.2. This gene was selected based on locus mapping from the array-comparative-genomic-hybridization (aCGH) data, and the known function of *KCTD13* as a substrate-specific adapter of the BCR (BTB-CUL3-RBX1) E3 ubiquitin-protein ligase complex. E3 ubiquitin ligases differentially regulate the androgen receptor (AR), which is required for the development and differentiation of male

genitalia by promoting AR transactivation by ubiquitination (RNF6 and Siah2), or inducing ubiquitin mediated degradation (MDM2 and CHIP)[15,16]. The E3 ubiquitin ligase complex also regulates the actin cytoskeleton and cell migration via ubiquitination and degradation of Ras Homolog Family Member A (RHOA), an important gene in sex determination[14,17,18]. Ubiquitination of proteins can signal their degradation, modify their activity or target them to specific membranes or cellular organelles[19]. This study shows that gene-dosage changes in *KCTD13* impact GU development through diminished nuclear AR.

METHODS

Study patient selection:

This study was approved by and is under the oversight of the Institutional Review Board at Baylor College of Medicine (BCM), Houston, TX. Human subject data and specimens were obtained following informed consent by the participants and/or his or her legally-authorized representative at Texas Children's Hospital (TCH). DNA from peripheral blood specimens from 76 patients with abnormal GU phenotypes was analyzed using two commercially available aCGH platforms: 3×720K from NimbleGen (Madison, WI) and CytoScan HD from Affymetrix (Santa Clara, CA). NimbleGen aCGH samples were processed at the Roche Service Lab in Iceland. Affymetrix aCGH samples were processed at the Fullerton Genetics Center (Asheville, NC). A sample of blood was obtained at the time of surgical intervention for their GU anomaly. Saliva samples were collected from the parents. DNA was extracted from all samples using the Qiagen Puregene DNA extraction kit (Valencia, CA) according to the manufacturer's protocol. Data were analyzed using Nexus-Copy-Number software from BioDiscovery (Hawthorne, CA). To validate the aCGH data, a TaqMan copy number (CNV) assay was run for KCTD13 (Hs01712568_cn) from Applied Biosystems (Foster City, CA). TaqMan CNV reactions were performed in triplicate as previously described[20]. Samples were analyzed using CopyCaller V2.1 software from Applied Biosystems. Statistical analysis was performed using Prism software from GraphPad (La Jolla, CA).

Creation of *Kctd13* haploinsufficient and null mice using CRISPR/Cas9 genome editing:

All experiments were executed in accordance with institutional guidelines and were approved by the Institutional Animal Care and Use Committee at Baylor College of Medicine. Mice were housed in a 12-hour light/12-hour dark cycle and received diet and water ad libitum. In collaboration with the BCM Mouse ES Cell and the Genetically Engineered Mouse Cores, CRISPR/Cas9 genome editing technology was used to successfully produce mice heterozygous for a *Kctd13* deleted allele (*Kctd13*$^{+/-}$). CRISPR-mediated mutagenesis, with guide RNAs targeting intronic sequences on either side of *Kctd13* exon 2, was used to delete the entirety of exon 2 by non-homologous end joining. Deletion of exon 2 in the resulting transcript induced a frameshift and a premature stop codon in exon 3, which is predicted to cause nonsense-mediated decay of the mutant transcript. Although CRISPR/Cas9 off-target mutagenesis is extremely rare *in vivo*[21–23], high-resolution melting analysis of the top five predicted off-target sites for each sgRNA was used to verify the absence of off-target effects. Importantly, guide RNA selection was prioritized so that potential off-target sites were located on chromosomes other than

chromosome 16; the location of *Kctd13*. Therefore, if a rare off-target mutagenesis event occurs, it is possible to segregate it from the *Kctd13* allele in one generation of breeding.

Phenotypic analyses of *Kctd13*-haploinsufficient, -null and wild-type mice:

Phenotyping of sexually mature homozygous, heterozygous, and WT mice was conducted at 8–10 weeks after birth (n=5). External genitalia and the entire urinary tract were dissected and evaluated for DSD. The animals were weighed prior to dissection. The position, size and appearance of penis, gubernaculum, testis, kidney, seminal vesicles, epididymis, urethra and ureter were recorded. Penises were fixed in 10% neutral buffered formalin overnight, and then preserved in 70% ethanol for 24h. Penises were photographed using light microscopy and then analyzed by microCT. For microCT analysis, penises were incubated overnight in an iodine solution (volumetric, 0.05 M I_2 (0.1N), Cat # 318981, Sigma Aldrich) and then embedded in 1% agarose. Specimens were scanned as previously described[24] using a μCT SKYSCAN 1272 scanner (Bruker Corporation, Billerica MA) at a resolution of 20μm. Cross-sectional images from tomography projection images were reconstructed to TIF files using the NRecon software. The cross-platform application HARP (Harwell Automated Reconstruction Processor, MRC Harwell, Didcot UK) was used for automating the processing of μCT image data. To analyze, process, and visualize penile structures, image data from HARP, the 3D Slicer software (http://www.slicer.org) was used. After testicular excision and weight calculation, one of the testes was submerged in Bouin's solution for five hours and then preserved in 70% ethanol. Specimens were processed, embedded in paraffin, sectioned, and then H&E or PAS-stained by the Histology & Pathology Core at the Baylor College of Medicine (HTAP is supported by the P30 Cancer Center Support Grant (NCI-CA125123). The other testis was flash-frozen and use for protein analysis. Epididymides were excised and then rinsed with modified HTF medium with gentamicin - HEPES (Cat # 90126, Irvine Scientific, Santa Ana CA). After being transferred to a clean 5ml tube, the epididymides were minced and then blended with 1ml of HTF medium. Sperm and testicular/epididymal secretions were obtained after an incubation for 30 minutes at 37°C, 5% CO_2. Sperm were allowed to swim, and genital tract secretions diffused out of the fragments. Sperm count, and motility data are not normally distributed and therefore expressed as median values (interquartile ranges 25th–75th percentile).

Cell culture:

A human cervical squamous cell carcinoma stable line expressing green fluorescent protein tagged androgen receptor (HeLa-AR-GFP biosensor) was kindly provided by Professor Michael A. Mancini (Baylor College of Medicine Houston, TX)[25]. Human embryonic kidney (HEK293) cells, human ureteric uroepithelial cells (SV-HUC-1), and human primary bladder smooth muscle cells (PCS-420–012) were purchased from American Type Culture Collection (Manassas, VA). Primary human foreskin fibroblasts (UD11) were obtained from a patient who underwent circumcision at TCH after IRB consent and approval. HeLa-AR-GFP cells were grown in DMEM-F12 (1:1) (Cat# 11330032,ThermoFisher), 10% FBS, Hygromycin (200 ug/ml) or phenol red-free DMEM media (Cat # 21063–029, ThermoFisher Scientific, Sugar Land TX) supplemented with 10% charcoal stripped and dialyzed fetal bovine serum (SD-FBS, Cat # MT35072CV, ThermoFisher Scientific), 1% of MEM non-essential amino acids (Cat # 11140–050, ThermoFisher Scientific), 1% of

GlutaMAX (Cat # 35050–061, ThermoFisher Scientific), and 500 μg/ml hygromycin (Cat # 10687010, ThermoFisher Scientific). HEK293 and UD11 were grown in 10% FBS supplemented DMEM (ThermoFisher Scientific). SV-HUC-1 were grown in 10% FBS supplemented F-12K medium. PCS-420–012 were grown in basal medium (ATCC Cat # PCS-100–030) supplemented with vascular smooth muscle cell growth kit (ATTCC Cat # PCS-100–030). All cells were maintained at 37°C and 5% CO_2 atmosphere.

Immunofluorescence in cells:

24 hours before the experiment, cells were grown on poly-D-lysine coated cover slips in 6-well-plates. Cells were rinsed with PBS and incubated for 1h with 10nM of R1881 (Cat # NLP005005MG, PerkinElmer, Akron OH). Cells were fixed with 4% paraformaldehyde for 10 minutes, rinsed with PBS three times, mounted on slides, and eventually were counterstained with DAPI (ProLong Diamond Antifade Mountant Medium with DAPI, Cat # P36962 ThermoFisher). Cells were examined for AR nuclear translocation under a Olympus BX51 Fluorescence Microscope and the associated software cellSens. Images for the GFP-AR HeLa cells were acquired with a Leica TCS SP8 confocal microscope. Individual cells were analyzed for the morphology of the nucleus and the number of cells with a hyperspeckled cyan nuclei, were counted using the cell counter tool of the software Image J. One-way ANOVA (multiple comparison) was used for statistical analysis on five independent experiments using GraphPad Prism software. Detection of KCTD13 in human urogenital derived cells *in vitro* was carried out by using KCTD13 rabbit polyclonal antibody (1:200, Cat # ab32974, Abcam Cambridge, MA) as per manufacturer's instructions. As a secondary antibody, the Goat anti-Rabbit IgG antibody, Alexa Fluor 488 Secondary antibody (1:1000, Cat # A270340, ThermoFisher Scientific), was used.

Knockdown of *KCTD13 In Vitro*:

To quantify the nuclear fraction of AR, HeLa-AR-GFP cells were grown to 70% confluence in 10cm-plates and were then mock-transfected with either 70nM of siRNA scramble (ON-TARGETplus Non-targeting Control Pool, GE Healthcare Life Science, Pittsburgh PA) or 70nM of siRNA-KCTD13 (ON-TARGETplus Human KCTD13 (253980) siRNA – SMARTpool, GE Healthcare Life Science). After 48h, some sets of plates were exposed to the synthetic androgen R1881 for 30 minutes while others were exposed to R1881 for 60 minutes. Then, cells were harvested, lysed, with RIPA buffer containing Complete™ EDTA-free Protease Inhibitor Cocktail (Cat # 4693132001, Sigma Aldrich), and protein concentration was determined by a Bradford assay. For protein nuclear extraction, the protocol from Abcam (https://www.abcam.com/protocols/nuclear-extraction-protocol-nuclear-fractionation-protocol) was used. The images presented are representative results of experiments that were repeated four times, using samples from different sets of HeLa-AR cell plates, and yielded similar results. For nuclear extraction the NE-PER Nuclear and Cytoplasmic Extraction Reagents kit (ThermoFisher Scientific) was used. Briefly, ice-cold CER I + protease inhibitor was added to the cell pellets, following the reagent volumes indicated in manufacturer's user guide. After vortexing the tube vigorously for 15 seconds to fully suspend the cell pellet, tubes were incubated on ice for 10 minutes. Ice-cold CER II was added to tubes, vortexed for 5 seconds, and incubated on ice for 1 minute. After that, tubes were centrifuged for 5 minutes at 16,000×g. Supernatant (cytoplasmic extract)

was immediately transferred to a clean pre-chilled tube and kept on ice. The insoluble pellet (nuclear extract) was suspended in ice-cold NER + protease inhibitor, and tubes were vortexed for 15 seconds. Then tubes were vortexed for 15 seconds every 10 minutes, for a total of 40 minutes. Tubes were centrifuged at 16,000×g for 10 minutes. Supernatant fraction was transferred to a clean pre-chilled tube and protein concentration was calculated by the Bradford method.

Protein detection:

For Western blot, 30μg of protein/lane was electrophoresed on 10% SDS-PAGE gels and blotted onto PVDF membranes (Immobilon-P, EMD Millipore, Billerica MA). For immunodetection the following primary antibodies were used: rabbit polyclonal antibody against KCTD13 (0.4μg/ml, Cat # HPA043524, Atlas Antibodies, Bromma, Sweden), rabbit polyclonal to AR (1:1000, Cat # A303–996A, Bethyl Laboratories, Montgomery, TX), rabbit polyclonal to GAPDH (1:1000, Cat # ab9485, Abcam), mouse monoclonal to ß-tubulin (1:1000, Cat # 2146, Cell Signaling Technology Inc.), rabbit monoclonal to SOX9 (1:500, Cat # ab185230, Abcam), rabbit polyclonal to PLZF (1.1000, Cat # ab39354, Abcam). Membranes were blocked, and antibodies were diluted according to manufacturer's instructions. Goat anti-mouse IgG (H + L)-HRP conjugate (1:1000, Cat #170–6516, BIORAD, Hercules CA); and goat anti-rabbit IgG (H + L)-HRP Conjugate (1:1000, Cat # 170–6515, BIORAD) secondary antibodies were used as per manufacturer's instructions. For the chemiluminescence reaction, the SuperSignal™ West Pico PLUS Chemiluminescent Substrate (Cat # 34580, ThermoFisher Scientific) was used. Images were acquired with the Chemidoc™ Touch Imaging System (Cat # 1708370, BIORAD) and its associated software Image Lab Touch version 1.2. Western blot band intensity was analyzed using the freely available software NIH Image J (http://imagej.nih.gov/ij/). For IHC, testis sections underwent heat-induced (98°C) epitope retrieval in 0.1M sodium citrate for 12 min. Tissue samples were deparaffinized and rehydrated in gradients of xylene and ethanol, then washed twice with PBS; tissue was permeabilized in 0.2% Triton X-100 in PBS for 30 min on a rotatory shaker. After washing, tissues were blocked 30 min in 5% normal blocking serum in PBS. For immunodetection, the following primary antibodies were used: rabbit polyclonal to KCTD13 (1:200, Atlas Antibodies), mouse monoclonal to AR (1:200, Cat # 554225, BD Biosciences, San Jose CA), rabbit monoclonal to SOX9 (1:200, Abcam); and goat polyclonal to PLZF for IHC (1:200) (Cat # AF2944, R & D Systems, Minneapolis MN). Primary antibodies were diluted in PBS plus 5% normal serum belonging to the same species in which the secondary antibody was raised. Samples were incubated overnight at 4°C in a humid chamber. On the following day, after washing, slides stained with SOX9 were incubated for 1h at room temperature in 5% donkey blocking serum in PBS containing donkey anti-rabbit IgG (H+L) highly cross-adsorbed secondary antibody, Alexa Fluor 555 (1:250, Cat # A- 31572, ThermoFisher Scientific). Slides were washed three times in PBS, counterstained, and mounted with VECTASHIELD Antifade Mounting Medium with DAPI. Slides stained with PLZF, after washing, were incubated for 40 min at room temperature with a biotinylated goat Anti-rabbit IgG Antibody (1:200 Cat # BA-1000, Vector Laboratories), washed again, and stained for 30 min with solution A&B (Cat # PK-6100, VECTASTAIN® Elite® ABC-HRP Kit, Vector Laboratories). Finally, DAB staining was performed (Cat # SK-4100, DAB peroxidase (HRP) Substrate Kit

(with Nickel), 3, 3'-diaminobenzidine) as per manufacturer's instructions. Slides were counterstained with Mayer's hematoxylin solution (Cat # MHS16 Sigma-Aldrich). For IHC, five WT males, and five *Kctd13*$^{-/-}$, all aged 8 weeks, were divided into control and experimental groups, respectively. From each animal, 30 seminiferous tubules in different stages were counted. Seminiferous tubule dimensions (from circular tubular cross sections) was defined using a circle drawn with Microsoft PowerPoint. The same sizes of circles were drawn for both WT and *Kctd13*$^{-/-}$ seminiferous tubules and their respective cell numbers were estimated. Sertoli cells and spermatogonial cell numbers were defined based upon their distinguishing and specific cell morphologic differences. The sections were examined at 400X and 1000X magnifications using an Olympus BX51 microscope and its associated software cellSens (Olympus, Tokyo Japan).

RESULTS

KCTD13 gene-dosage changes are significantly increased in patients with GU anomalies

Using aCGH, our laboratory identified two boys with GU birth defects with CNVs at 16p11.2 that encompassed *KCTD13*[4,7]. The first individual carried a *de novo* 131 kb microdeletion at the 16p11.2 locus, which encompassed *KCTD13*, and who had hypospadias and a cleft palate[4]. The second patient had a ~600 kb paternally-inherited duplication in this region and exhibited hypospadias, cryptorchidism, and micropenis[7]. The minimal 131 kb deleted region at 16p11.2 encoded nine candidate genes, while the more commonly observed 16p11.2 microduplication/microdeletion syndrome region includes 27 genes; *KCTD13* was present in both types of CNVs[4]. After screening 271 patients with GU anomalies using quantitative polymerase chain reaction (qPCR), five additional patients with CNVs in *KCTD13* (one duplication and four deletions) were identified (Figure 1A–C). In a large screening cohort study of 6813 patients, the occurrence rate of CNVs within 16p11.2 in the general population was very low (0.10%), with only two deletions and five duplications recorded in the small CNV in 16p11.2 encompassing *KCTD13*[26]. The incidence of CNVs in *KCTD13* in individuals with GU defects was significantly different for duplications (p=0.026) and for deletions (p=0.0001) by Fisher Exact Test when compared to the general population as described by Tucker *et al.*,[26] (Figure 1C). Congenital GU anomalies in these five patients included both upper and lower tract anomalies (vesicoureteral reflux (VUR), ureteropelvic junction obstruction (UPJO), hypospadias, and cryptorchidism) (Figure 1A). CNVs in *MAZ*, a gene within this minimal 16p.11.2 region contributes to upper tract GU anomalies and other birth defects[7]. Of the seven individuals identified with *KCTD13* CNVs, only four were male. The two boys carrying *KCTD13* duplications both had cryptorchidism, and one also had hypospadias. Of the five individuals with a deletion, two were males; one of them had bilateral cryptorchidism and the other had isolated hypospadias. All males with *KCTD13* CNVs in the cohort had external genitalia defects. No *KCTD13* defects were identified in the 198 individuals without congenital GU anomalies tested in the laboratory (Figure 1C).

A review of the literature and public databases revealed over 30 patients with defects in *KCTD13* and concomitant GU anomalies[4,6–11,27–30]. GU anomalies identified in this group of patients included upper and lower GU tract anomalies, such as multicystic dysplastic

kidneys (MCDK), VUR, ectopic testes, and ambiguous genitalia. Phenotypic and genotypic data using the web-based database DatabasE of genomiC variation and Phenotype in Humans using Ensembl Resources (DECIPHER; https://decipher.sanger.ac.uk) identified 643 patients sharing variants in *KCTD13*, including 247 females, 358 males, and 38 patients labeled "other" or "unknown"[31]. Phenotype information was available from 437 patients (male and females) with the majority (136) having intellectual disability. Although GU birth defects are not always described in this database, 16 boys had GU defects that involved the genitalia, including one male with hypoplastic external genitalia, seven with cryptorchidism, five with hypospadias, and three with micropenis. Also, there were six individuals with kidney abnormalities including 2 boys with renal agenesis[31].

KCTD13 is robustly expressed in the mouse and human urinary tract

To define the role and expression profile of *Kctd13* in mouse embryonic GU tract development, *in situ* hybridization (ISH) was performed. ISH revealed robust expression of *Kctd13* in the entire GU tract, especially in the genital tubercle in E13.5 and E15.5 mouse embryos (Figure 2A, B). Immunohistochemical staining of sagittal sections of developing mouse genital tubercle showed strong KCTD13 expression in the urethra, epithelial lamina, and preputial glands (Figure 2F, G). This expression persists through adulthood, and is observed in adult penile urethra and epithelia lamina (Figure 2H, I). In fetal and postnatal testis, KCTD13 is expressed in the testis chords and seminiferous tubules respectively (Figure 2K, L). In the adult testis, KCTD13 is expressed both in the seminiferous tubules as well as the Leydig cells. In the seminiferous tubules, KCTD13 expression is present in both Sertoli and germ cells. Within the germ cells, KCTD13 is present in both spermatocytes and round spermatids, but the expression is lacking in elongated spermatids (Figure 2M–N). Immunofluorescent staining of mouse Sertoli cells (TM4) also displayed strong endogenous cytoplasmic KCTD13 expression (Figure 2E). Immunofluorescent staining from the human GU tract derived cell line SV-HUC1 (ureteric-uroepithelial cells) exhibited strong endogenous cytoplasmic KCTD13 expression (Figure 2D).

KCTD13 loss impacts androgen receptor (AR) ligand-dependent nuclear sub-cellular localization.

A functional AR and AR signaling pathway are required for the development and differentiation of male genitalia. AR is differentially regulated by a variety of E3 ubiquitin ligases with some E3 ubiquitin ligases enhancing AR transcriptional activation activity and others leading to AR degradation[15,16]. While *KCTD13* encodes a substrate-specific adapter of the BCR E3 ubiquitin-protein ligase complex, the effect of *KCTD13* gene-dosage changes on AR function or expression was unknown. To elucidate the effect of gene-dosage changes of *KCTD13* on AR function, a HeLa cell line stably expressing wild-type GFP-AR herein called HeLa-AR cells[25] was employed. In HeLa-AR cells, in the absence of androgen, the GFP-AR is diffusely distributed predominantly in the cytoplasm. However, after the addition of synthetic non-metabolizable androgen, R1881, most of the cytoplasmic AR-fluorescent marker translocates to the nucleus where it exhibits a hyperspeckled pattern[25]. After *KCTD13* knockdown, AR levels in HeLa-AR cells were measured in the presence of R1881, or absence of ligand (ethanol-treated, vehicle control). Western blot analysis showed a transient decrease in nuclear fraction of AR level at short intervals after treatment with

androgen in the HeLa-AR cells with *KCTD13* knockdown (Figure 3B). This significant decrease in nuclear AR localization was further demonstrated by immunofluorescent analysis of GFP-AR expression pattern in HeLa cells after the addition of R1881. Nuclear translocation in HeLa-AR cells was quantified with and without *KCTD13* knockdown by counting the proportion of cells showing minimal or no GFP in the cytoplasm and nuclear hyperspeckled (H) pattern indicating translocation of GFP-tagged AR versus cells showing no translocation with GFP present mainly in the cytoplasm (Figure 3C). In control cells (siScramble), prior to the addition of R1881, most cells exhibited GFP-AR localization in the cytoplasm (Figure 3C–1). However, the addition of R1881 caused GFP-AR translocation in 80% of the analyzed cells within 60 min (Figure 3C–2). Interestingly, the percentage of HeLa-AR cells showing nuclear translocation was significantly reduced to only 38% in 60 min after *KTCD13* knockdown, indicating a significant reduction in AR translocation in the absence of *KTCD13* (Figure 3C–4). These results indicate that *KCTD13* gene-dosage changes impact AR translocation, which may in turn contribute to the undervirilized phenotype seen in humans with 16p11.2 CNVs encompassing this gene. AR mRNA levels were unchanged when *KCTD13* knockdown was performed in HeLa-AR cells, indicating that *KCTD13* does not affect *AR* expression (Figure 3A).

Kctd13 null male mice are sub-fertile

To define *Kctd13* function *in vivo*, a *Kctd13* mouse model (*Kctd13*$^{-/-}$) was produced using CRISPR/Cas9-mediated mutagenesis targeting the murine *Kctd13* exon 2. Deletion of the *Kctd13* exon 2 induced a frameshift in the transcript, which introduced a premature stop codon in exon 3 predicted to cause a nonsense-mediated decay of the mutant transcript. Sanger sequencing confirmed this deletion of Exon 2 (Figure 4A). According to the database proteinatlas.org, the organ with the highest expression of KCTD13 is the testis; however, this gene is widely expressed throughout many parts of the body. Accordingly, Western blot analysis of testicular extracts was performed to corroborate the lack of KCTD13 in null mice (Figure 4B). Immunohistochemistry was performed in testicular sections from wild-type (WT) and *Kctd13*$^{-/-}$ mice to determine the testicular cellular expression. In WT mice, KCTD13 was present mainly in the nuclei of germ cells but was not present in sperm. The somatic cells of the testis, including Sertoli and interstitial cells, also express KCTD13 (Figures 2M and 4C). No staining is observed in the testes of *Kctd13*$^{-/-}$ mice (Figures 2O and 4C). *Kctd13*$^{-/-}$ mice are viable, and since their neurological phenotype was recently described[14,32], the current investigation focused on understanding the role of this gene in GU defects, the second most common defect observed in patients with CNVs encompassing *KCTD13*.

The fertility and fecundity of *Kctd13*$^{-/-}$ mice was defined and their external genitourinary tract examined for phenotypic anomalies. Male *Kctd13*$^{-/-}$ mice were sub-fertile compared to WT (control) males and produced a significantly lower number of litters in a six-month period (seven mating cycles of 25 days each) when mated with WT females (Figure 5). WT males normally sired seven litters during seven mating cycles. However, the five *Kctd13*$^{-/-}$ male mice studied produced significantly fewer litters: two produced three litters, two produced four litters and one produced five litters (Figure 5A). The average days between litters for *Kctd13*$^{-/-}$ male mice were also significantly greater than the number of days

between pregnancies in WT mice ($p<0.001$) (Figure 5B). The cumulative number of pups produced was significantly smaller in the *Kctd13*$^{-/-}$ group than that in the WT group. The five WT male mice produced 263 pups with an average of 7.51±1.04 pups per litter and a litter size ranging from 6–10 pups per litter. In contrast, the five *Kctd13*$^{-/-}$ males sired a total of 93 pups with an average of 4.89±1.29 pups per litters with litter sizes ranging from 3–8 pups per litter ($p<0.001$) (Figure 5C–D). Analysis of sperm retrieved from the epididymis of *Kctd13*$^{-/-}$ mice identified a significant decrease in sperm concentration and motility in these mice when compared to WT mice ($p \leq 0.05$), which likely contributes the subfertility observed (Figure 6F).

Testicular anomalies are present in male *Kctd13* null and haploinsufficient mice

Similar to the birth defects present in patients with CNVs encompassing *KCTD13*, phenotypic analysis of *Kctd13*$^{-/-}$ mice revealed a significantly greater frequency of cryptorchidism than present in WT mice. *Kctd13*$^{-/-}$ and *Kctd13*$^{+/-}$ male mice exhibited a gene dosage-dependent increase in cryptorchidism rates of 57.14% (12/21) and 33.33% (7/21), respectively, compared to the (1/21; 4.76%) rate observed in WT mice ($p \leq 0.05$) (Figure 6E). In the *Kctd13*$^{-/-}$ group, 33.33% had unilateral and 23.8% had bilateral cryptorchidism. Similarly, in the *Kctd13*$^{+/-}$ group, 19.04% had unilateral and 14.28% had bilateral cryptorchidism, indicating a dosage-dependent increase in cryptorchidism with decreased *Kctd13* copy number. There was no significant difference in laterality of cryptorchidism between the heterozygous and null mice. Testes of *Kctd13* mutant mice were smaller than that of WT mice, regardless of being cryptorchid (Figure 6D, F). The average testis weight in *Kctd13*$^{-/-}$ was 72.04mg compared to 103.95mg in WT mice ($p \leq 0.05$). *Kctd13*$^{-/-}$ mice also exhibited significantly decreased epididymal and seminal vesicle weights when compared with WT mice (Figure 6F). No significant differences in serum testosterone, FSH, or LH levels of adult WT and *Kctd13* mutant male mice were observed (Figure 6F).

Histological analysis of testes from the *Kctd13*$^{-/-}$ mice showed no overt defect in spermatogenesis at two months of age (Figure 7B). However, as these mice aged, missing generations of germ cells were evident in testis histology (Figure 7C). To determine if there was a decrease in specific cell-types within the seminiferous epithelium, spermatogonia and Sertoli cells were quantified using immunohistochemistry and Western blot. A Sertoli cell marker, SOX9, and a pan-undifferentiated spermatogonial cell marker, PLZF, were used to assess spermatogenesis in two-month old mice (sexually mature age). Compared to WT mice, the total number of Sertoli cells per seminiferous tubule cross-section was significantly decreased in *Kctd13*$^{-/-}$ mice (Figure 7G–I). This correlated with significantly decreased levels of SOX9 in the testis of *Kctd13*$^{-/-}$ mice (Figure 7M–N). AR, predominantly expressed in Sertoli and peritubular cells, also showed significantly reduced levels in mutant mice when compared to WT mice (Figure 7D–F and M–N). Since each Sertoli cell can only support a limited number of germ cells and the mutant mice have fewer Sertoli cells per cross-section, the number of spermatogonia were quantified. The total number of PLZF-positive spermatogonia was significantly decreased in the seminiferous tubule cross-sections of *Kctd13*$^{-/-}$ mice compared to that in WT mice (Figure 7J–L), which correlated with significantly decreased levels of PLZF seen on Western blot analysis in the

total mouse testis of *Kctd13*$^{-/-}$ mice (Figure 7M–N). It also corresponded to the decreased levels of Sertoli cells in the seminiferous epithelium.

Kctd13 null mice exhibit penile anomalies

Penises of *Kctd13*$^{-/-}$ mice were considerably smaller than those of WT mice (Figure 8A). To quantify differences in penile structure, the penile morphology of mutant and WT mice was defined using MicroCT[24]. MicroCT analysis revealed significantly reduced penile lengths in *Kctd13*$^{-/-}$ mice compared to those in WT mice (Figure 8–D). By definition, a micropenis measures ≥2.5 standard deviations (SD) below the mean penile length for a given age. The average penile length in WT mice was 5.88±0.16mm. A penile length below 5.48mm would therefore be considered a micropenis in our mouse cohort. The length of 15 *Kctd13*$^{-/-}$ mouse penises ranged from 2.90–5.54 mm with 13/15 penises characterized as micropenises. Sixty percent of null mouse penises had a length below 4mm (11.5SD). We evaluated additional penile parameters (Figure 9) to determine if the global penile development was affected. When compared to WT mice, the male urogenital mating protuberance (MUMP) length was significantly shorter in null mice (Figure 9A–C). The baculum (the bone in the murine penis) length and base width were significantly shorter and narrower respectively in null mice compared to those in WT mice (Figure 9D–I). While the penises of mutant mice were smaller, the urethral meatus location was similar and orthotopic in location in both mutant and WT penises.

Since individuals with 16p11.2 CNVs had upper GU tract defects[4–14], the kidneys of null mice were examined. None of the WT mice displayed kidney abnormalities (n=21). Most *Kctd13* mutant mice had normal kidneys. One incidental finding was the presence of unilateral upper pole hydronephrosis in one null and one heterozygous mouse (data not shown; n=21).

DISCUSSION

In humans, the 16p11.2 microdeletion/microduplication syndrome is characterized by a wide array of developmental and intellectual anomalies. While advances have been realized with respect to defining the genetic basis of neurological disorders found in patients with 16p11.2 microdeletion/microduplication syndrome, our understanding of the genes involved in the GU anomalies observed with this syndrome remains unclear. This work identified a minimal overlap region at 16p11.2 in patients with GU anomalies consisting of 8 complete genes (*PRRT2, PAGR1, MVP, CDIPT, CDIPT-AS1, SEZ6L2, ASPHD1, KCTD13*) and a portion of one gene (*MAZ*). The probability of loss of function intolerance (pLI) score is the probability that a given gene falls into the haploinsufficient category. The pLI was very low for all these genes (below 0.50), with the exception of *KCTD13* (pLI 0.79) and *MAZ* (pLI 0.95). From these genes, the two more highly expressed in the GU tract were *KCTD13* and *MAZ*, with the expression of the other seven genes in the GU tract being moderate to low according to GUDMAP database[33]. *PRRT2, PAGR1, MVP, CDIPT, CDIPT-AS1, SEZ6L2, ASPHD1* are associated with neurological disorders and cancer among other diseases, but not with any GU defects[34–39]. All these finding suggest that *KCTD13* and *MAZ* are most plausible to cause the range of different GU phenotypes observed in these patients.

In our recently published study on the role of *MAZ* (MYC-associated zinc finger transcription factor) gene-dosage changes in human urogenital development and the phenotype of mice deficient in *Maz*[7], we hypothesized that MAZ competes with WT-1 to impact WNT signaling to cause GU anomalies. *Maz*-deficient mice exhibited a dose-dependent lethality with haploinsufficient mice being viable and the null mice exhibiting fetal lethality. Diminished *MAZ* expression resulted in differential expression of several *Wnt* morphogens required for normal GU development, including *Wnt11* and *Wnt4*[7]. As we hypothesized given the importance of WT-1 to human GU development, haploinsufficiency of *Maz* in the mouse model revealed a high penetrance of upper urinary tract anomalies, including hydronephrosis, renal agenesis and renal dysplasia, as well as decreased bladder weight and capacity, demonstrating that *Maz* is an important gene in upper GU tract development[7]. Of note, this *Maz* null mouse model could not be used to define the role of *Maz* in testicular descent, because testicular descent in mice occurs after birth. Thus, this cryptorchidism could be not assessed due to the high incidence of post-natal lethality of *Maz*-null mice.

Given the wide-spread expression of KCTD13 in the GU tract and the importance of the E3 ubiquitin-protein ligase complex in the regulation of androgen receptor transcriptional activation and degradation, as well as effects on cellular architecture, motility, and proliferation, *KCTD13* was the second plausible candidate gene at 16p11.2 hypothesized to be critical for normal GU development. While the incidence of defects in *KCTD13* in the general population is low at 0.10%, the rate of CNVs in patients with GU anomalies (2.58%; 7/271) is significantly elevated when compared to patients without GU anomalies (0/198). Importantly, *KCTD13* gene dosage changes in the male study group appeared to be exclusively associated with penile and/or testicular defects.

The current study reveals that loss of *Kctd13* in a mouse model impacted androgen receptor nuclear localization and signaling *in vitro* and *in vivo*. AR is a member of the steroid receptor superfamily that is required for the normal development and differentiation of the male GU tract. Abnormalities of AR expression, sub-cellular localization or function result in a wide spectrum of GU birth defects, including severe hypospadias or complete sex reversal[40–42]. Androgen Insensitivity Syndrome (AIS), resulting from abnormalities of AR protein structure, expression, sub-cellular localization or function, is an example of a disorder of sexual differentiation (DSD) in which AR mutations results in partial or complete feminization of the male external genitalia including testicular and penile development[43]. AIS is a recognized, albeit fairly uncommon, cause of under-virilization of a 46, XY male. In the presence of androgen, AR nuclear translocation and occupancy are required for AR signaling[44]. After KCTD13 knockdown *in vitro*, nuclear AR levels were decreased suggesting that KCTD13 plays an important role in nuclear occupancy affecting either translocation or AR degradation[15,16]. AR translocation to the nucleus requires an intact microtubular cytoskeleton, which is potentially regulated by E3 ubiquitin ligases[45]. Since E3 ubiquitin ligases mediate AR degradation, it is possible that loss of KCTD13 in mutant mice results in increased AR degradation, which could also contribute to the undervirilized phenotype seen in both humans and mice. In the absence of efficient nuclear AR translocation or enhanced AR degradation in *KCTD13* haploinsufficient humans and *Kctd13* deficient mice, the reduced AR nuclear localization and action may explain in part

the undervirilized phenotype observed leading to GU defects that affect the fertility of these mice.

In the testis, total testicular AR levels are diminished *in vivo* compared with wild-type control testes, but this is because there are less Sertoli present in *KCTD13*-deficient testis. Sertoli and peritubular myoid cells are the major cell types expressing AR in the seminiferous tubules. More importantly, *Kctd13* null mice had smaller and cryptorchid testes with reduced number of spermatogonia and Sertoli cells in *Kctd13* null mice may also contribute to the subfertility of the *Kctd13 null* mice. *Kctd13* null mice have smaller epididymides. In an androgen-deprived condition, the cellular architecture and function of the epididymis, which is exquisitely androgen responsive, is altered[46]. Decreased AR signaling due to the lack of KCTD13 in the epididymis may impair its function, affecting sperm maturation and leading to lower sperm motility and subfertility. The lower AR nuclear occupancy together with the lower numbers of Sertoli cells and spermatogonia collectively contributed to lower sperm concentration and diminished epididymal function as assessed by lowered sperm motility.

Androgen and AR signaling are an important regulator of penile length[47]. The *Kctd13* null mouse exhibited a smaller epididymis and phallus with reduced baculum width and length that can be attributed to diminished AR nuclear occupancy. This reduced size could further contribute to the subfertility of *Kctd13* null mouse because a diminutive mouse baculum is correlated with reduced litter size[48].

AR activity is regulated to a great degree by posttranslational modifications, such as phosphorylation, acetylation, SUMOylation, and ubiquitination[49]. The ubiquitination-deubiquitination cycle of AR is complex since there are several E3 ubiquitin ligases involved in this cycle that can play distinct roles. Ubiquitination of AR by the E3 ligase CHIP[50,51], or Mdm2[52] promotes AR degradation by the 26S proteasome. The E3 ubiquitin ligase Parkin modulates polyQ-expanded AR levels[51]. The ubiquitin E3 ligase, RNF6, induces AR ubiquitination and promotes AR transcriptional activity in prostate cancer[53]. Angelman syndrome results from a defect in the E6-AP ubiquitin-proteosome protein degradation pathway of nuclear receptors including AR[54]. The deubiquitinases USP10, USP26, and USP12 interact with AR and regulate its function and signaling[55–57]. USP7 interacts with AR, mediates its deubiquitination, and facilitates the binding of AR to chromatin in prostate cancer cells as well as reduced mutant AR aggregation and cytotoxicity in cell models of spinal and bulbar muscular atrophy (SBMA)[58]. The regulation of AR by such E3 ligases is complex and the role of CUL3-KCTD13 in modulating AR for proper development of the GU tract remains unclear. Nevertheless, it is possible that the ubiquitin-mediated modulation of AR axis contributes to the under virilized phenotype observed in both humans and mice. *Cul3* regulates cytoskeleton protein homeostasis and cell migration in brain development[59] and a similar mechanism can occur in the GU tract.

KCTD13 gene dosage changes also have direct effects on other genes involved in sexual differentiation. Two critical genes associated with disorders of sexual differentiation (DSD) are *SOX9*[60,61] and *MAP3K1*[62,63]. Lack of SOX9 nuclear translocation induces DSD[64]. *MAP3K1* gain of function mutations can cause DSD abnormalities by decreasing *SOX9*

activity[62,63]. SOX9 is expressed in the gubernaculum and it modulates the INSL3 pathway, which is required for testicular descent[65,66]. SOX9 is expressed in the genital tubercle and in the urethral epithelium[67].

Although hypospadias was not observed in *Kctd13*$^{-/-}$ mice, 87% of *Kctd13*$^{-/-}$ mice had micropenis. KCTD13 is present at high levels in the urethra, corpus cavernosum and the epithelial lamina of developing and adult mouse penises. The epithelial lamina forms the prepuce and glans epithelium of the penis[68]. The internal preputial epithelial lamina plays a critical role in penile length determination as it detaches the glans from the external prepuce allowing the phallus to extend to its normal length[68]. Therefore, in the absence of KCTD13, maldevelopment of the internal prepuce could occur, affecting phallus extension leading to micropenis. Dihydrotesterone (DHT), a 5-alpha reduced androgen is the testosterone metabolite that is required for AR binding in many tissues, plays an essential role in penile lengthening[69]. Therefore, KCTD13 mediated AR signaling is potentially an important determinant of penile length.

This study shows that patients with GU birth defects, previously thought to be non-syndromic, may harbor other phenotypic anomalies associated with copy number changes of syndromic regions like the 16p11.2 microdeletion/microduplication syndrome. The identification of *KCTD13* as a dosage-sensitive regulator of lower GU development and *MAZ* as a gene predominantly affecting upper tract GU development in the 16p11.2 microdeletion/microduplication syndrome region[7] point to the importance of understanding the role of these proteins in both upper and lower GU development. Finally, the well characterized signaling mechanism in genitalia development involving AR and SOX9 seem to be influenced by KCTD13 to ensure proper GU development.

Supplementary Material

Refer to Web version on PubMed Central for supplementary material.

Acknowledgments

This study was supported in part by The National Institutes of Health Multidisciplinary K12 Urologic Research (KURe) Career Development Program K12DK0083014 from the National Institute of Digestive Diseases and Kidney to D.J.L (AS, SL and CJJ were K12 scholars), R01DK078121 from the National Institutes of Health, National Institute of Digestive Diseases and Kidney to DJL, and 1R01HD100985 from the Eunice Kennedy Shriver National Institute of Child Health and Human Development to AS and CJJ and the Society for Pediatric Urology annual research award (2017) to AS. MO was a pre-doctoral trainee supported on T32DK007763 (to DJL). DJL is also supported in part by the Frederick J. and Theresa Dow Wallace Fund of the New York Community Trust. We thank Drs. Francesco DeMayo and Jason Heaney at the Baylor College of Medicine's GEM core for their assistance in generating the *Kctd13* deleted mice and Dr. Victor Ruthig, Ms. Adlai Nelson and Carolyn Schum for helpful editing of the manuscript. The Optical Imaging and Vital Microscopy core used in this project was supported by the Integrated Microscopy Core at Baylor College of Medicine with funding from the NIH (DK56338, and CA125123), CPRIT (RP150578), the Dan L. Duncan Comprehensive Cancer Center, and the John S. Dunn Gulf Coast Consortium for Chemical Genomics).

Data Availability Statement

All relavant data generated by this study is available withing the manuscript.

REFERENCES

1. Hughes IA Early management and gender assignment in disorders of sexual differentiation. Endocrine development 11, 47–57, doi:10.1159/0000111057 (2007). [PubMed: 17986826]
2. Pohl HG, Joyce GF, Wise M & Cilento BG Jr. Cryptorchidism and hypospadias. The Journal of urology 177, 1646–1651, doi:10.1016/j.juro.2007.01.058 (2007). [PubMed: 17437777]
3. Kolon TF et al. Evaluation and Treatment of Cryptorchidism: AUA Guideline. J Urol, doi:10.1016/j.juro.2014.05.005 (2014).
4. Tannour-Louet M et al. Identification of de novo copy number variants associated with human disorders of sexual development. PLoS One 5, e15392, doi:10.1371/journal.pone.0015392 (2010). [PubMed: 21048976]
5. Itsara A et al. Population analysis of large copy number variants and hotspots of human genetic disease. Am J Hum Genet 84, 148–161, doi:S0002–9297(09)00002–0 [pii] 10.1016/j.ajhg.2008.12.014 (2009). [PubMed: 19166990]
6. Sampson MG et al. Evidence for a recurrent microdeletion at chromosome 16p11.2 associated with congenital anomalies of the kidney and urinary tract (CAKUT) and Hirschsprung disease. Am J Med Genet A 152A, 2618–2622, doi:10.1002/ajmg.a.33628 (2010). [PubMed: 20799338]
7. Haller M, Au J, O'Neill M & Lamb DJ 16p11.2 transcription factor MAZ is a dosage-sensitive regulator of genitourinary development. Proc Natl Acad Sci U S A 115, E1849–E1858, doi:10.1073/pnas.1716092115 (2018). [PubMed: 29432158]
8. Nik-Zainal S et al. High incidence of recurrent copy number variants in patients with isolated and syndromic Mullerian aplasia. J Med Genet 48, 197–204, doi:10.1136/jmg.2010.082412 (2011). [PubMed: 21278390]
9. Jacquemont S et al. Mirror extreme BMI phenotypes associated with gene dosage at the chromosome 16p11.2 locus. Nature 478, 97–102, doi:10.1038/nature10406 (2011). [PubMed: 21881559]
10. Kino T et al. ZNF764 haploinsufficiency may explain partial glucocorticoid, androgen, and thyroid hormone resistance associated with 16p11.2 microdeletion. J Clin Endocrinol Metab 97, E1557–1566, doi:10.1210/jc.2011-3493 (2012). [PubMed: 22577170]
11. Shinawi M et al. Recurrent reciprocal 16p11.2 rearrangements associated with global developmental delay, behavioural problems, dysmorphism, epilepsy, and abnormal head size. J Med Genet 47, 332–341, doi:10.1136/jmg.2009.073015 (2010). [PubMed: 19914906]
12. Golzio C et al. KCTD13 is a major driver of mirrored neuroanatomical phenotypes of the 16p11.2 copy number variant. Nature 485, 363–367, doi:10.1038/nature11091 (2012). [PubMed: 22596160]
13. Kusenda M et al. The Influence of Microdeletions and Microduplications of 16p11.2 on Global Transcription Profiles. Journal of child neurology 30, 1947–1953, doi:10.1177/0883073815602066 (2015). [PubMed: 26391891]
14. Escamilla CO et al. Kctd13 deletion reduces synaptic transmission via increased RhoA. Nature 551, 227, doi:10.1038/nature24470 https://www.nature.com/articles/nature24470#supplementary-information (2017). [PubMed: 29088697]
15. Qi J et al. The E3 ubiquitin ligase Siah2 contributes to castration-resistant prostate cancer by regulation of androgen receptor transcriptional activity. Cancer Cell 23, 332–346, doi:10.1016/j.ccr.2013.02.016 (2013). [PubMed: 23518348]
16. Rees I, Lee S, Kim H & Tsai FT The E3 ubiquitin ligase CHIP binds the androgen receptor in a phosphorylation-dependent manner. Biochim Biophys Acta 1764, 1073–1079, doi:10.1016/j.bbapap.2006.03.013 (2006). [PubMed: 16725394]
17. Chen Y et al. Cullin mediates degradation of RhoA through evolutionarily conserved BTB adaptors to control actin cytoskeleton structure and cell movement. Molecular cell 35, 841–855, doi:10.1016/j.molcel.2009.09.004 (2009). [PubMed: 19782033]
18. Ostrer H Disorders of sex development (DSDs): an update. J Clin Endocrinol Metab 99, 1503–1509, doi:10.1210/jc.2013-3690 (2014). [PubMed: 24758178]

19. Lin DH et al. ROMK1 channel activity is regulated by monoubiquitination. Proceedings of the National Academy of Sciences of the United States of America 102, 4306–4311, doi:10.1073/pnas.0409767102 (2005). [PubMed: 15767585]
20. Jorgez CJ et al. Aberrations in Pseudoautosomal Regions (PARs) Found in Infertile Men with Y-Chromosome Microdeletions. J Clin Endocrinol Metab 94, 674–679, doi:jc.2010-2018 [pii] 10.1210/jc.2010-2018 (2011).
21. Yang H, Wang H & Jaenisch R Generating genetically modified mice using CRISPR/Cas-mediated genome engineering. Nature protocols 9, 1956–1968, doi:10.1038/nprot.2014.134 (2014). [PubMed: 25058643]
22. Yang H et al. One-step generation of mice carrying reporter and conditional alleles by CRISPR/Cas-mediated genome engineering. Cell 154, 1370–1379, doi:10.1016/j.cell.2013.08.022 (2013). [PubMed: 23992847]
23. Shen B et al. Efficient genome modification by CRISPR-Cas9 nickase with minimal off-target effects. Nature methods, doi:10.1038/nmeth.2857 (2014).
24. O'Neill M, Huang GO & Lamb DJ Novel Application of Micro-Computerized Tomography for Morphologic Characterization of the Murine Penis. J Sex Med 14, 1533–1539, doi:10.1016/j.jsxm.2017.10.065 (2017). [PubMed: 29153581]
25. Szafran AT, Szwarc M, Marcelli M & Mancini MA Androgen receptor functional analyses by high throughput imaging: determination of ligand, cell cycle, and mutation-specific effects. PLoS One 3, e3605, doi:10.1371/journal.pone.0003605 (2008). [PubMed: 18978937]
26. Tucker T et al. Prevalence of selected genomic deletions and duplications in a French-Canadian population-based sample of newborns. Molecular genetics & genomic medicine 1, 87–97, doi:10.1002/mgg3.12 (2013). [PubMed: 24498606]
27. Shinawi M et al. Mixed gonadal dysgenesis in a child with isodicentric Y chromosome: Does the relative proportion of the 45,X line really matter? American journal of medical genetics. Part A 152A, 1832–1837, doi:10.1002/ajmg.a.33475 (2010). [PubMed: 20583182]
28. Rosenfeld JA et al. Speech delays and behavioral problems are the predominant features in individuals with developmental delays and 16p11.2 microdeletions and microduplications. Journal of neurodevelopmental disorders 2, 26–38, doi:10.1007/s11689-009-9037-4 (2010). [PubMed: 21731881]
29. Bijlsma EK et al. Extending the phenotype of recurrent rearrangements of 16p11.2: deletions in mentally retarded patients without autism and in normal individuals. Eur J Med Genet 52, 77–87, doi:10.1016/j.ejmg.2009.03.006 (2009). [PubMed: 19306953]
30. Hernando C et al. Comparative genomic hybridisation shows a partial de novo deletion 16p11.2 in a neonate with multiple congenital malformations. J Med Genet 39, E24 (2002). [PubMed: 12011165]
31. Firth HV et al. DECIPHER: Database of Chromosomal Imbalance and Phenotype in Humans Using Ensembl Resources. Am J Hum Genet 84, 524–533, doi:10.1016/j.ajhg.2009.03.010 (2009). [PubMed: 19344873]
32. Arbogast T et al. Kctd13-deficient mice display short-term memory impairment and sex-dependent genetic interactions. Hum Mol Genet 28, 1474–1486, doi:10.1093/hmg/ddy436 (2019). [PubMed: 30590535]
33. Davies JA et al. Access and use of the GUDMAP database of genitourinary development. Methods in molecular biology 886, 185–201, doi:10.1007/978-1-61779-851-1_17 (2012). [PubMed: 22639262]
34. Zhou L et al. Absence of association between major vault protein (MVP) gene polymorphisms and drug resistance in Chinese Han patients with partial epilepsy. J Neurol Sci 358, 362–366, doi:10.1016/j.jns.2015.09.363 (2015). [PubMed: 26476776]
35. Vlaskamp DRM et al. PRRT2-related phenotypes in patients with a 16p11.2 deletion. European journal of medical genetics, doi:10.1016/j.ejmg.2018.08.002 (2018).
36. Kumar A et al. Loss of function of mouse Pax-Interacting Protein 1-associated glutamate rich protein 1a (Pagr1a) leads to reduced Bmp2 expression and defects in chorion and amnion development. Developmental dynamics : an official publication of the American Association of Anatomists 243, 937–947, doi:10.1002/dvdy.24125 (2014). [PubMed: 24633704]

37. Kaur J et al. Clinical significance of phosphatidyl inositol synthase overexpression in oral cancer. BMC cancer 10, 168, doi:10.1186/1471-2407-10-168 (2010). [PubMed: 20426864]
38. Konyukh M et al. Variations of the candidate SEZ6L2 gene on Chromosome 16p11.2 in patients with autism spectrum disorders and in human populations. PLoS One 6, e17289, doi:10.1371/journal.pone.0017289 (2011). [PubMed: 21394203]
39. Ishikawa N et al. Characterization of SEZ6L2 cell-surface protein as a novel prognostic marker for lung cancer. Cancer Sci 97, 737–745, doi:10.1111/j.1349-7006.2006.00258.x (2006). [PubMed: 16863507]
40. Bouty A, Ayers KL, Pask A, Heloury Y & Sinclair AH The Genetic and Environmental Factors Underlying Hypospadias. Sexual development : genetics, molecular biology, evolution, endocrinology, embryology, and pathology of sex determination and differentiation 9, 239–259, doi:10.1159/000441988 (2015). [PubMed: 26613581]
41. Zheng Z, Armfield BA & Cohn MJ Timing of androgen receptor disruption and estrogen exposure underlies a spectrum of congenital penile anomalies. Proc Natl Acad Sci U S A 112, E7194–7203, doi:10.1073/pnas.1515981112 (2015). [PubMed: 26598695]
42. Tannour-Louet M et al. Increased gene copy number of VAMP7 disrupts human male urogenital development through altered estrogen action. Nat Med 20, 715–724, doi:10.1038/nm.3580 (2014). [PubMed: 24880616]
43. Hornig NC et al. Identification of an AR Mutation-Negative Class of Androgen Insensitivity by Determining Endogenous AR Activity. The Journal of clinical endocrinology and metabolism 101, 4468–4477, doi:10.1210/jc.2016-1990 (2016). [PubMed: 27583472]
44. Bennett NC, Gardiner RA, Hooper JD, Johnson DW & Gobe GC Molecular cell biology of androgen receptor signalling. Int J Biochem Cell Biol 42, 813–827, doi:10.1016/j.biocel.2009.11.013 (2010). [PubMed: 19931639]
45. Srivastava D & Chakrabarti O Mahogunin-mediated alpha-tubulin ubiquitination via noncanonical K6 linkage regulates microtubule stability and mitotic spindle orientation. Cell death & disease 5, e1064, doi:10.1038/cddis.2014.1 (2014). [PubMed: 24556679]
46. Robaire B & Hamzeh M Androgen action in the epididymis. Journal of andrology 32, 592–599, doi:10.2164/jandrol.111.014266 (2011). [PubMed: 21764895]
47. Fu XH, Zhang WQ & Qu XS Correlation of androgen receptor and SRD5A2 gene mutations with pediatric hypospadias in 46, XY DSD children. Genetics and molecular research : GMR 15, 15018232, doi:10.4238/gmr.15018232 (2016). [PubMed: 27051040]
48. Stockley P et al. Baculum morphology predicts reproductive success of male house mice under sexual selection. BMC biology 11, 66, doi:10.1186/1741-7007-11-66 (2013). [PubMed: 23800051]
49. Wen S, Niu Y & Huang H Posttranslational regulation of androgen dependent and independent androgen receptor activities in prostate cancer. Asian J Urol 7, 203–218, doi:10.1016/j.ajur.2019.11.001 (2020). [PubMed: 33024699]
50. He B et al. An androgen receptor NH2-terminal conserved motif interacts with the COOH terminus of the Hsp70-interacting protein (CHIP). J Biol Chem 279, 30643–30653, doi:10.1074/jbc.M403117200 (2004). [PubMed: 15107424]
51. Morishima Y et al. CHIP deletion reveals functional redundancy of E3 ligases in promoting degradation of both signaling proteins and expanded glutamine proteins. Hum Mol Genet 17, 3942–3952, doi:10.1093/hmg/ddn296 (2008). [PubMed: 18784277]
52. Lin HK, Wang L, Hu YC, Altuwaijri S & Chang C Phosphorylation-dependent ubiquitylation and degradation of androgen receptor by Akt require Mdm2 E3 ligase. EMBO J 21, 4037–4048, doi:10.1093/emboj/cdf406 (2002). [PubMed: 12145204]
53. Xu K et al. Regulation of androgen receptor transcriptional activity and specificity by RNF6-induced ubiquitination. Cancer Cell 15, 270–282, doi:10.1016/j.ccr.2009.02.021 (2009). [PubMed: 19345326]
54. Nawaz Z et al. The Angelman syndrome-associated protein, E6-AP, is a coactivator for the nuclear hormone receptor superfamily. Mol Cell Biol 19, 1182–1189, doi:10.1128/MCB.19.2.1182 (1999). [PubMed: 9891052]

55. Burska UL et al. Deubiquitinating enzyme Usp12 is a novel co-activator of the androgen receptor. J Biol Chem 288, 32641–32650, doi:10.1074/jbc.M113.485912 (2013). [PubMed: 24056413]
56. Dirac AM & Bernards R The deubiquitinating enzyme USP26 is a regulator of androgen receptor signaling. Molecular cancer research : MCR 8, 844–854, doi:10.1158/1541-7786.MCR-09-0424 (2010). [PubMed: 20501646]
57. Faus H, Meyer HA, Huber M, Bahr I & Haendler B The ubiquitin-specific protease USP10 modulates androgen receptor function. Mol Cell Endocrinol 245, 138–146, doi:10.1016/j.mce.2005.11.011 (2005). [PubMed: 16368182]
58. Pluciennik A et al. Deubiquitinase USP7 contributes to the pathogenicity of spinal and bulbar muscular atrophy. J Clin Invest 131, doi:10.1172/JCI134565 (2021).
59. Morandell J et al. Cul3 regulates cytoskeleton protein homeostasis and cell migration during a critical window of brain development. Nature communications 12, 3058, doi:10.1038/s41467-021-23123-x (2021).
60. Wirth J et al. Translocation breakpoints in three patients with campomelic dysplasia and autosomal sex reversal map more than 130 kb from SOX9. Hum Genet 97, 186–193 (1996). [PubMed: 8566951]
61. Wagner T et al. Autosomal sex reversal and campomelic dysplasia are caused by mutations in and around the SRY-related gene SOX9. Cell 79, 1111–1120 (1994). [PubMed: 8001137]
62. Pearlman A et al. Mutations in MAP3K1 cause 46,XY disorders of sex development and implicate a common signal transduction pathway in human testis determination. Am J Hum Genet 87, 898–904, doi:10.1016/j.ajhg.2010.11.003 (2010). [PubMed: 21129722]
63. Loke J et al. Mutations in MAP3K1 tilt the balance from SOX9/FGF9 to WNT/beta-catenin signaling. Hum Mol Genet 23, 1073–1083, doi:10.1093/hmg/ddt502 (2014). [PubMed: 24135036]
64. Argentaro A et al. A SOX9 defect of calmodulin-dependent nuclear import in campomelic dysplasia/autosomal sex reversal. The Journal of biological chemistry 278, 33839–33847, doi:10.1074/jbc.M302078200 (2003). [PubMed: 12810722]
65. Feng S et al. INSL3/RXFP2 signaling in testicular descent. Ann N Y Acad Sci 1160, 197–204, doi:10.1111/j.1749-6632.2009.03841.x (2009). [PubMed: 19416188]
66. Tomiyama H, Hutson JM, Truong A & Agoulnik AI Transabdominal testicular descent is disrupted in mice with deletion of insulinlike factor 3 receptor. J Pediatr Surg 38, 1793–1798, doi:10.1016/j.jpedsurg.2003.08.047 (2003). [PubMed: 14666470]
67. Sreenivasan R et al. Altered SOX9 genital tubercle enhancer region in hypospadias. The Journal of steroid biochemistry and molecular biology 170, 28–38, doi:10.1016/j.jsbmb.2016.10.009 (2017). [PubMed: 27989796]
68. Phillips TR, Wright DK, Gradie PE, Johnston LA & Pask AJ A Comprehensive Atlas of the Adult Mouse Penis. Sex Dev 9, 162–172, doi:10.1159/000431010 (2015). [PubMed: 26112156]
69. Sasaki G et al. Effects of pre- and post-pubertal dihydrotestosterone treatment on penile length in 5alpha-reductase type 2 deficiency. Endocr J, doi:10.1507/endocrj.EJ19-0111 (2019).

A

ID #	Gender	Mutation	Phenotype	Mode of inheritance
501 (aCGH)	Male	Duplication	Hypospadias+UDT	Paternally (Haller *et al.*, 2018)
579	Male	Duplication	UDT	Unknown
500 (aCGH)	Male	Deletion	Hypospadias	*De novo* (Tannour-Louet *et al.*, 2010)
596	Male	Deletion	UDT	Unknown
757	Female	Deletion	VUR	Unknown
908	Female	Deletion	UPJO	Unknown
1181	Female	Deletion	VUR	Unknown

B

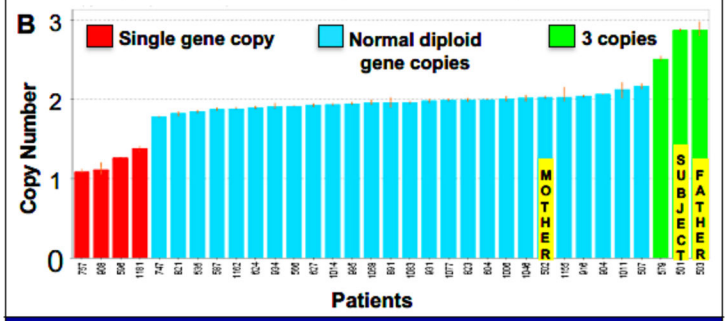

C General population CNV in *KCTD13* region according to Tucker *et al.*, 2013

Total	Normal (2X)	Deletion (≤ 1X)	Duplication (≥ 3X)	CNV frequency
6813	6806	2	5	0.10%

Individuals without GU abnormalities tested by qPCR for *KCTD13* CNV

Total	Normal (2X)	Deletion (≤ 1X)	Duplication (≥ 3X)	CNV frequency
198	198	0	0	0%

Individuals with GU abnormalities tested by qPCR for *KCTD13* CNV

Total	Normal (2X)	Deletion (≤ 1X)	Duplication (≥ 3X)	CNV frequency
271	264	5	2	2.58%*

Figure 1. Patients with CNVs in *KCTD13* gene at 16p11.2 exhibit lower genitourinary tract anomalies.

A) Characteristics of the individuals with CNVs in *KCTD13*. **B)** Results of TaqMan Copy Number Assay confirmed the microduplication in panel A (green bar) and showed that this was a paternally inherited CNV since the father had a duplication (green bar) and the mother had 2-copies of the gene (blue bar). This graph also shows the identification of four additional patients with microdeletions and one additional patient with a microduplication. Single gene copy (1X, **red**), two gene copies (2X, **blue**), and three or more gene copies (3+X, **green**). **C**) Comparison of the incidence of *KCTD13* CNV in our population of individuals with and without GU defects and in the general population as described by Tucker *et al.*, $p<0.0001$[26].

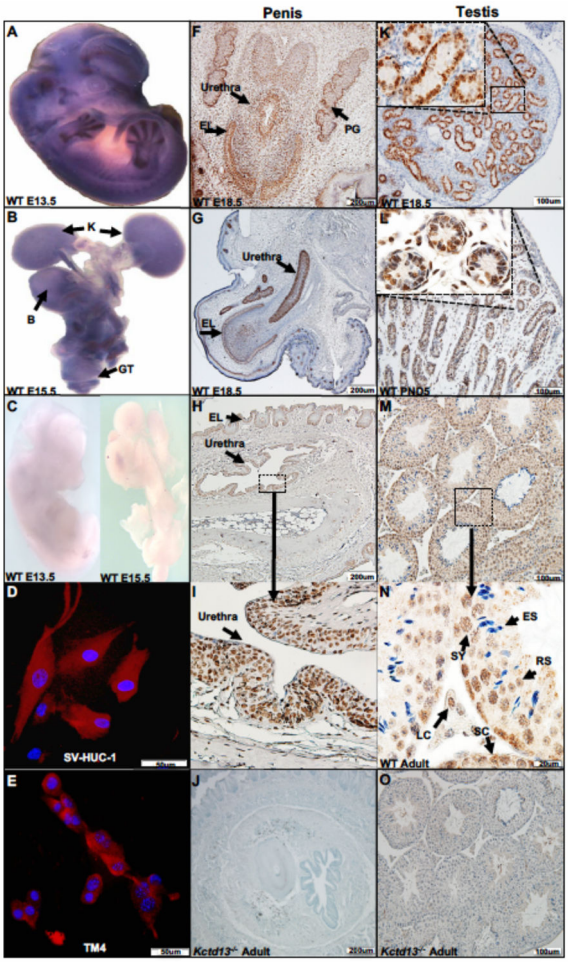

Figure 2. KCTD13 is highly expressed in the mouse GU tract and human GU cell lines.

A-B) *In situ* hybridization (ISH) with *Kctd13* antisense probes showed ubiquitous staining throughout E13.5 mouse embryos (**A**, blue staining) and micro-dissected E15.5 GU tracts (**B**, blue staining) indicating kidney (K), genital tubercle (GT), and bladder (B). **C)** Hybridization with *Kctd13* sense control probes exhibited minimal non-specific background staining. **D**) Immunofluorescence (IF) of human ureteric uroepithelial cells (SV-HUC-1) showed robust cytoplasmic KCTD13 expression (red). The cell nucleus was stained with DAPI (blue). **E**) IF of mouse Sertoli cell line TM4 showed robust cytoplasmic KCTD13 expression. **F-G)** Immunohistochemistry (IHC) of mouse genital tubercle (GT) at embryonic E18.5 indicated KCTD13 expression in the urethra, epithelia lamina (EL) and preputial glands (PG). **H-I)** IHC of mouse penis indicated KCTD13 expression in the urethra. **J)** IHC of *Kctd13*$^{-/-}$ mouse penis lacked KCTD13 expression in the urethra. **K)** IHC of mouse E18.5 testis indicated KCTD13 expression inside the testis chords **L)** IHC of PND5 testis from a WT mouse with robust KCTD13 expression inside the seminiferous tubules and some interstitial cells. **M-N**) IHC of adult WT testis with expression in Sertoli cells (SC), Leydig cells (LC) and spermatocytes (SY). Elongated spermatids (ES) are negative and round spermatids (RS) have minimal expression. **O)** IHC of *Kctd13*$^{-/-}$ mouse adult testis lacked KCTD13 expression.

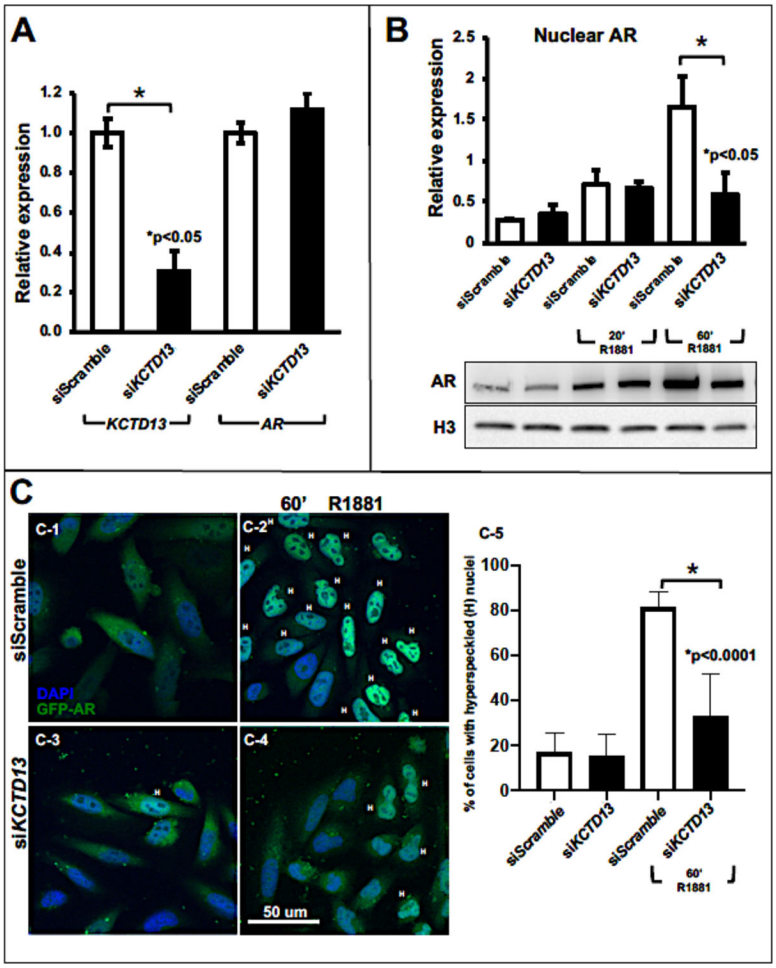

Figure 3. ***KCTD13*** **knockdown in HeLa-AR cells show reduced nuclear androgen receptor (AR) levels.**

A) After *KCTD13* knockdown (si*KCTD13*) in HeLa-AR cells, mRNA levels of *KCTD13* decreased by 69.5% but AR mRNA levels did not change. **B)** Nuclear extracts from HeLa-AR cells showed decreased AR nuclear levels with *KCTD13* knockdown (si*KCTD13*) after acute exposure to R1881 when compared to cells treated with siScramble. Data are presented as means±s.e.m. of four different experiments and were analyzed using a paired-samples t-test using GraphPad Prism **C)** Immunofluorescent imaging of HeLa-AR-GFP cells confirmed decreased nuclear GFP-AR levels in cells treated with acute R1881 for 60 minutes (scale bars, 50 μm). Nuclear translocation was evaluated using the expression of GFP-AR either in the nucleus or cytoplasm of the cells, as well as the subnuclear AR speckles features. In both the siScramble (C-1) and si*KCTD13* (C-3) controls, the nuclei are predominantly blue, and the green is observed mostly in the cytoplasm. The addition of R1881 resulted in the absence of green in the cytoplasm and a cyan hyperspeckled nuclei (H) indicative of the movement of the AR to the nuclei in the majority of the siScramble HeLa-AR-GFP cells (C-2), but not in the siKCTD13 HeLa-AR-GFP cells (C-4). The images shown are representative results of five independent experiments; all individual experiments yielded similar results. Quantification of the data (C-5) are presented as mean ± standard

error of the mean and were analyzed using One way ANOVA (multiple comparison) using GraphPad Prism (GraphPad Software, Inc, La Jolla, CA, USA).

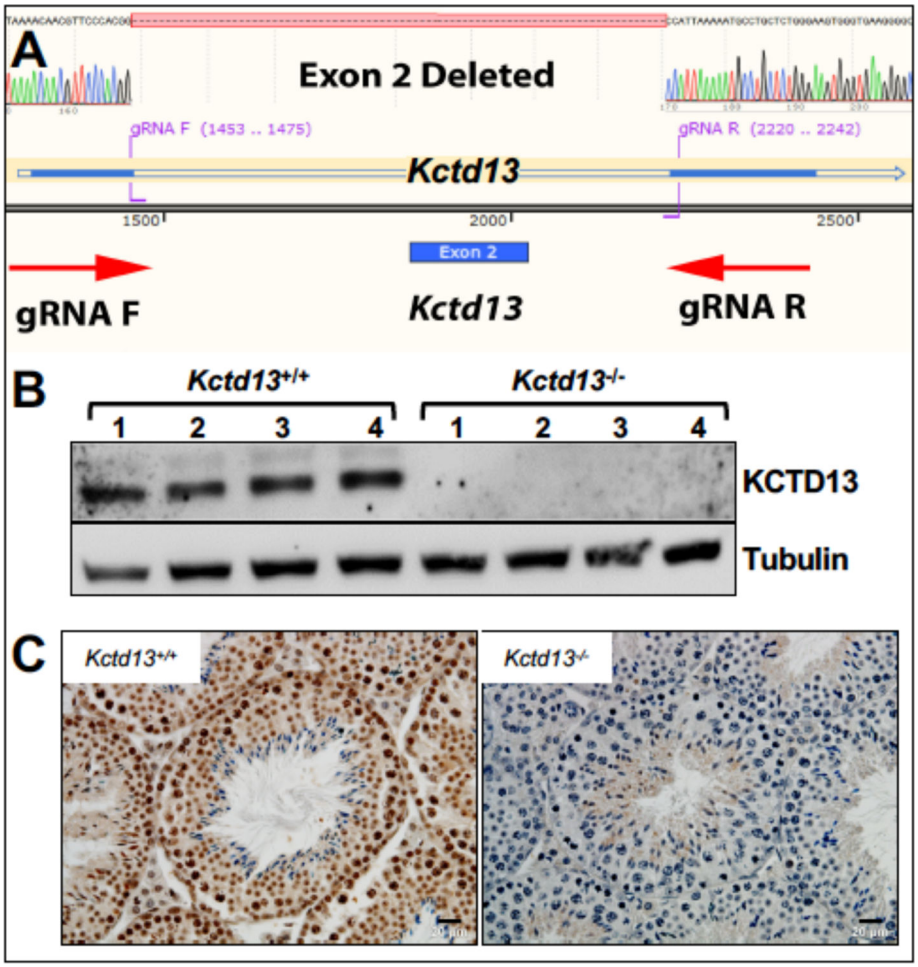

Figure 4: KCTD13 is not present in the testes of *Kctd13*$^{-/-}$ mice generated using CRISPR/Cas9 genome editing.

A) Sanger sequencing of a *Kctd13*$^{-/-}$ mouse tail indicated the deletion of the whole exon 2. **B)** Western blot analysis of testes extracts from WT and *Kctd13*$^{-/-}$ mice showed the KCTD13 band is present in all WT mice and absent in *Kctd13*$^{-/-}$ mice. β-tubulin was used as an internal control. **C)** Immunohistochemistry of testicular sections from WT mice indicated high KCTD13 expression (brown staining) in the nucleus of spermatogonia, spermatocytes and round spermatids. Sertoli and interstitial cells were also positive. The sperm were negative (blue staining). No staining was observed in the testis of *Kctd13*$^{-/-}$ mice.

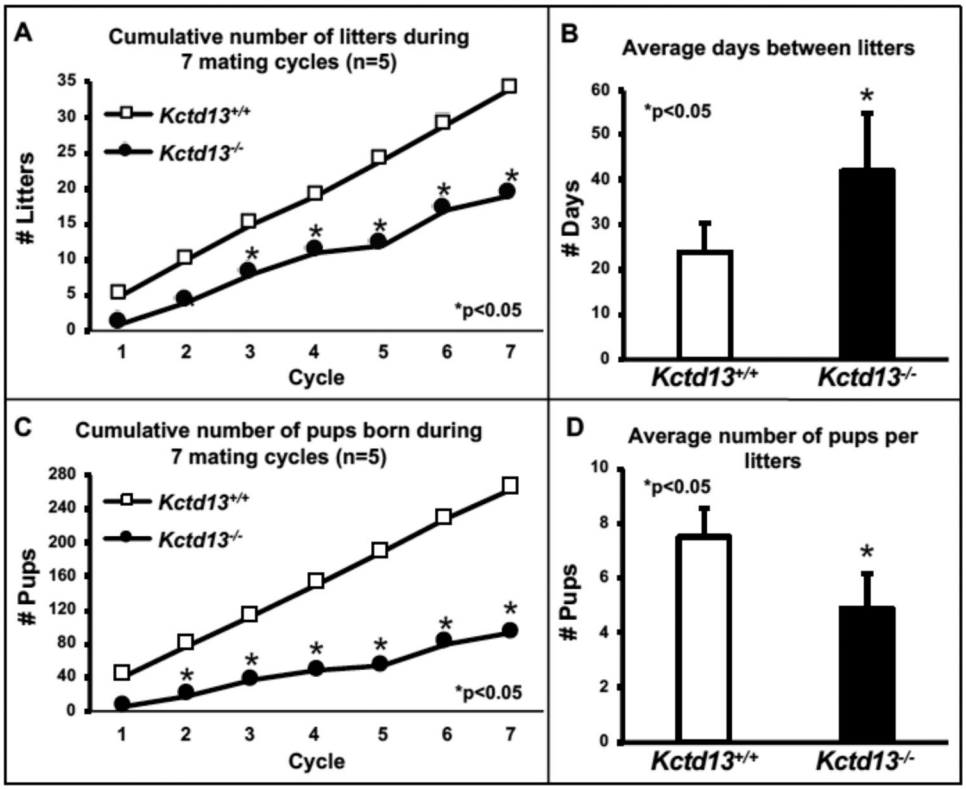

Figure 5: *Kctd13*$^{-/-}$ mice are subfertile.

A-B) The cumulative number of litters produced by five WT male mice each mated repeatedly to individual WT females during 7 mating cycles (25 days) was 34 with an average of 23.89±6.44 days between litters. In contrast, the cumulative number of litters produced by five *Kctd13*$^{-/-}$ male mice mated to a WT female during the same time was 19 with an average of 42.00±12.83 days between litters, p<0.001. **C-D**) The cumulative number of pups produced by five WT male mice mated to a WT female during 7 mating cycles (25 days) was 263 with an average of 7.51±1.04 pups per litter. In contrast, the cumulative number of pups produce by five *Kctd13*$^{-/-}$ male mice each mated to individual WT females during the same period was 93 with an average of 4.89±1.29 pups per. *p<0.001.

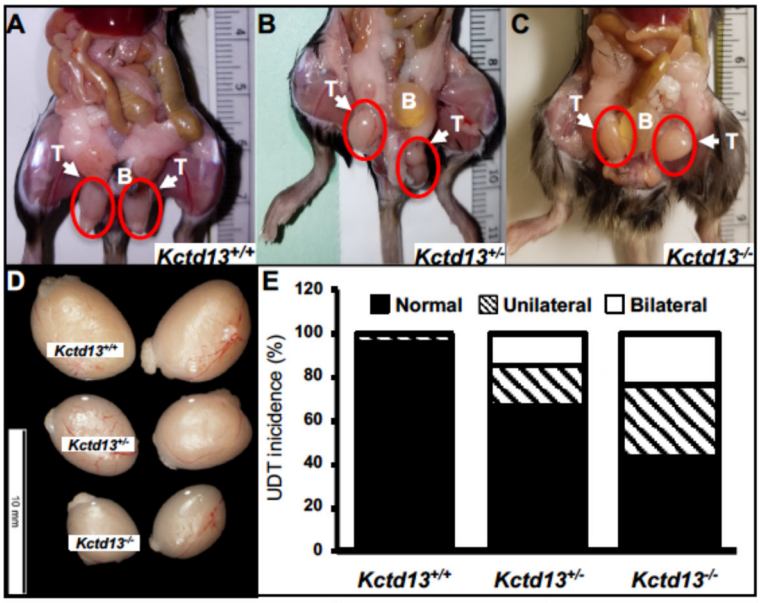

F Characteristics	*Kctd13*$^{+/+}$	*Kctd13*$^{-/-}$
Testicular weight (mg)	103.95 ± 6.13	72.04 ± 4.89*
Epididymal weight (mg)	50.10 ± 3.00	35.56 ± 1.38*
Seminal vesicle weight (mg)	387.48 ± 61.78	251.83 ± 6.64*
Sperm count (10^7)	2.05 ± 0.12	1.14 ± 0.10*
Sperm motility (%)	62.50 ± 6.16	17.00 ± 8.73*
Serum testosterone (ng/dL)	413.23 ± 711.89	296.42 ± 267.61
Serum FSH (ng/mL)	40.27 ± 8.41	47.68 ± 12.14
Serum LH (ng/mL)	1.62 ± 1.86	2.50 ± 1.21

Figure 6: Decreased AR action in *Kctd13* mutant mice manifested with a significant decrease in testis, epididymis and seminal vesicles weights, and increased rate of cryptorchidism.

A) WT mouse with normally positioned testes (T) in the scrotum, the bladder (B) is shown and provides a landmark. **B)** *Kctd13*$^{+/-}$ mouse with right UDT. **C)** *Kctd13*$^{-/-}$ mouse with bilaterally undescended testes above the inguinal ring at the level of the bladder. **D)** Testis size varied according to *Kctd13* gene dosage with *Kctd13*$^{-/-}$ mice having significantly smaller testes (Scale bars, 10 mm). **E)** Frequency of cryptorchidism (UDT) is significantly increased in *Kctd13*$^{-/-}$ and *Kctd13*$^{+/-}$ mice compared to WT mice, n=21. **F)** *Kctd13*$^{-/-}$ mice show a significant reduction in testicular, epidydimal, and seminal vesical weights. A significant decrease in sperm number and motility was also determined. A Mann-Whitney-Wilcoxon test indicated that sperm motility was greater for WT than for *Kctd13*$^{-/-}$ mice (Median=62.5 and Median=17 respectively, p = 0.0001), and sperm count was greater in WT than *Kctd13*$^{-/-}$ mice (Median=10.3 and Median= 5.6, respectively, p = 0.0022).

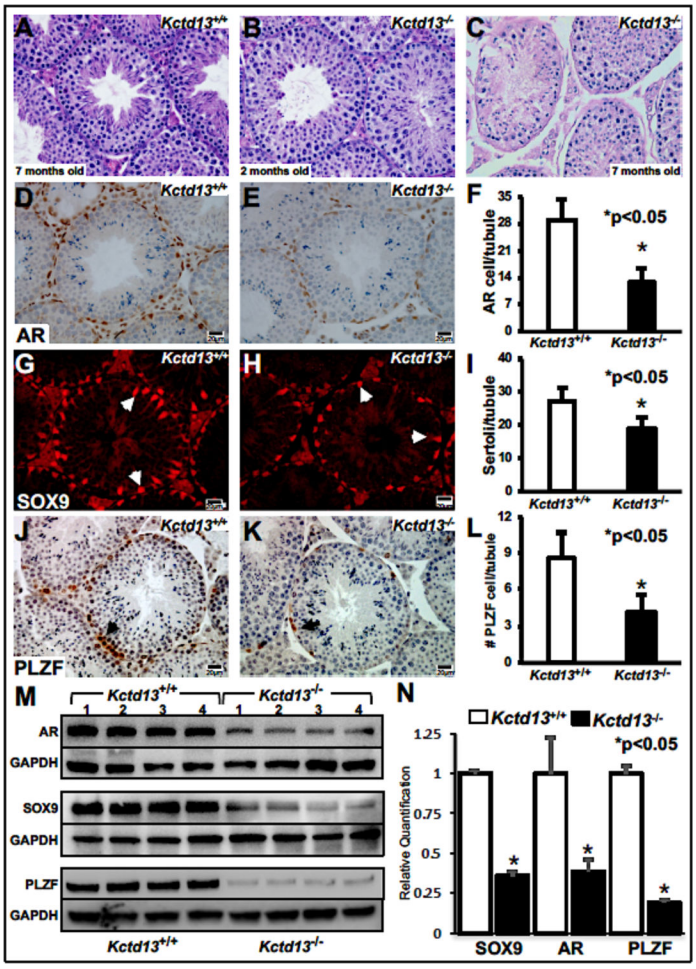

Figure 7. Testis of *Kctd13*$^{-/-}$ mice exhibit multiple abnormalities.

A-C) PAS staining of WT mice at 7 months of age (**A**), and *Kctd13*$^{-/-}$ mice at 2 months of age (**B**) and 7 month of age (**C**). No major difference noted between mice in panels A and B; however, *Kctd13*$^{-/-}$ mice at 7 months have abnormal seminiferous tubules with disorganized spermatogenesis. **D-E)** Detection of AR in testes of two-month-old WT and *Kctd13*$^{-/-}$ mice, respectively, showed significantly reduced AR levels in mutant mice. **F)** Graph depicts a 56% mean reduction in the number of AR-positive cells per tubule cross-section in five *Kctd13*$^{-/-}$ mice compared to five WT mice. **G-H)** Two-month-old WT mice exhibited greater SOX9 expression compared to *Kctd13*$^{-/-}$ mice. White arrows show localization of Sertoli cells in seminiferous tubules. **I)** Graph showing 32% mean reduction of Sertoli cells per tubule cross-section in five *Kctd13*$^{-/-}$ mice compared to five WT mice. **J-K)** Detection of pan-undifferentiated spermatogonial marker PLZF in testes of five WT and five *Kctd13*$^{-/-}$ two-month-old mice respectively, showed reduced levels present in mutant mice. Black arrows show localization of spermatogonia in seminiferous tubules (Scale bars, 20 μm). **L)** Graph showing 42% reduction of spermatogonia per tubule cross-section in five *Kctd13*$^{-/-}$ mice compared to five WT mice. **M)** Western blot analysis showed significant decreases of AR, SOX9, and PLZ, in the testes of *Kctd13*$^{-/-}$ mice compared to WT mice. Additional mice were tested in each group for a total of twelve mice per group (data not shown). **N)**

Graph represents quantitative analysis of Western blot of AR, SOX9, and PLZF proteins. Graph is showing relative expression ratio compared to GAPDH from twelve WT and twelve *Kctd13*$^{-/-}$ mouse testes. The images shown are representative results of experiments that were repeated using samples from different sets of animals and yielded similar results. Data presented as means±SD *$p<0.05$.

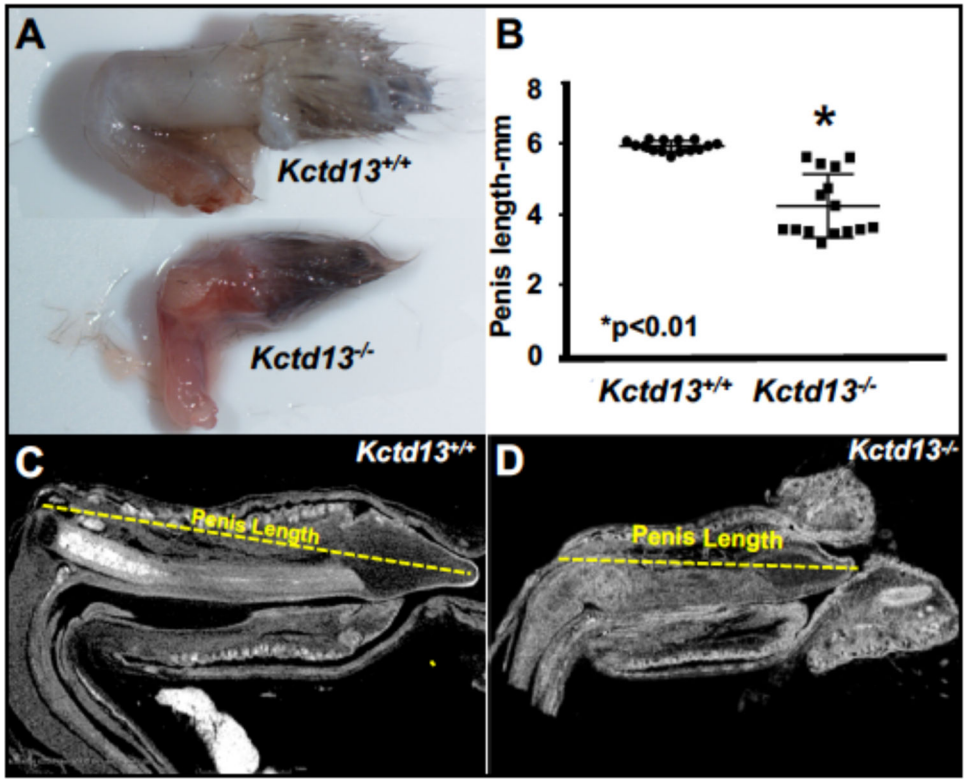

Figure 8. ***Kctd13*$^{-/-}$ mice exhibit micropenis.**

A) *Kctd13*$^{-/-}$ mice had shorter penises than those in WT mice. **B-D**) Penile length of mutant and WT mice assessed via micro-CT imaging revealed significantly reduced penile length in *Kctd13*$^{-/-}$ mice (mean 4.04±0.97mm) compared to WT mice (mean 5.88±0.16mm). The length of 15 *Kctd13*$^{-/-}$ mice penises ranged from 2.90–5.54mm. Data are presented as means±SD. *p<0.01. Dimensions in the graphs are expressed in mm. Data (mean ± SEM) were analyzed using Student t-test assuming equal variances using GraphPad Prism. A *P* value of less than .05 was considered statistically significant.

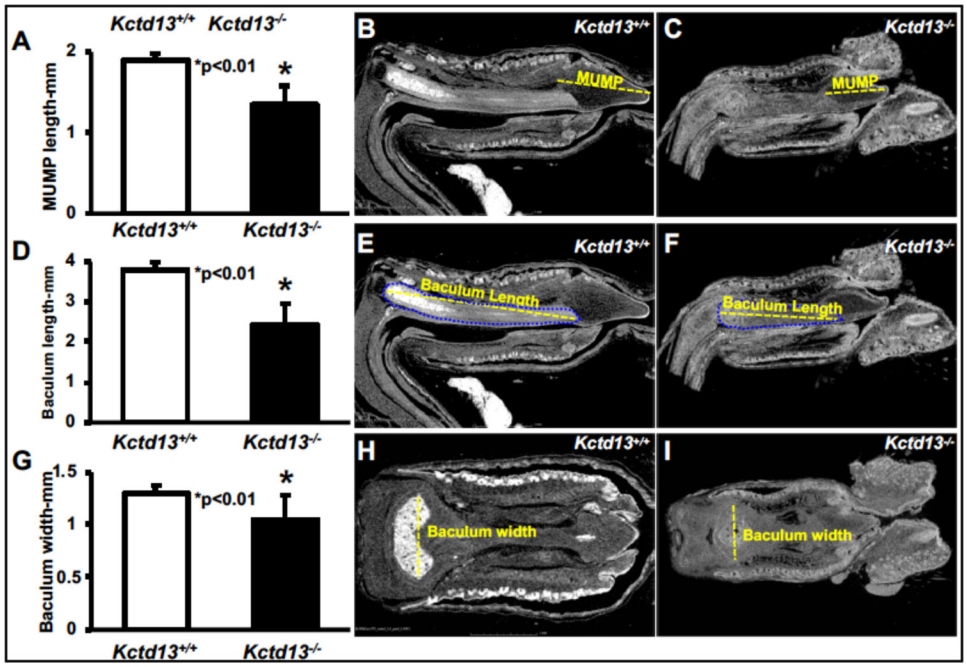

Figure 9. ***Kctd13*$^{-/-}$ mice exhibit several penile abnormalities.**

A-C) Penile morphology of mutant and WT mice assessed via micro-CT imaging indicated that Kctd13 null mice had a significantly shorter MUMP since *Kctd13*$^{-/-}$ mice had a mean MUMP length of 1.25±0.16mm and the WT mice had a mean MUMP length of 1.98±0.18mm. **D-F)** The mean baculum length of *Kctd13*$^{-/-}$ and WT mice were 2.91±0.71mm and 3.99±0.09mm, respectively. **G-I)** The mean baculum width was significantly smaller and narrower in null mice 0.97±0.16mm compared to WT mice width of 1.32±0.08mm. Data are presented as means±SD. *p<0.05. Dimensions in the graphs are expressed in mm. Data (mean ± SEM) were analyzed using Student t-test assuming equal variances using GraphPad Prism. A *P* value less than 0.05 was considered statistically significant.